



HAL
open science

Corrosion of pure and milled Mg₁₇Al₁₂ in “model” seawater solution

Serge Al Bacha, Isabelle Aubert, O. Devos, Mirvat Zakhour, Michel Nakhl,
Jean-Louis Bobet

► **To cite this version:**

Serge Al Bacha, Isabelle Aubert, O. Devos, Mirvat Zakhour, Michel Nakhl, et al.. Corrosion of pure and milled Mg₁₇Al₁₂ in “model” seawater solution. *International Journal of Hydrogen Energy*, 2020, 45 (32), pp.15805-15813. 10.1016/j.ijhydene.2020.04.030 . hal-02874725

HAL Id: hal-02874725

<https://hal.science/hal-02874725>

Submitted on 19 Jun 2020

HAL is a multi-disciplinary open access archive for the deposit and dissemination of scientific research documents, whether they are published or not. The documents may come from teaching and research institutions in France or abroad, or from public or private research centers.

L'archive ouverte pluridisciplinaire **HAL**, est destinée au dépôt et à la diffusion de documents scientifiques de niveau recherche, publiés ou non, émanant des établissements d'enseignement et de recherche français ou étrangers, des laboratoires publics ou privés.

Corrosion of pure and milled Mg₁₇Al₁₂ in “model” seawater solution

S. Al Bacha ^{a,b,c}, I. Aubert ^c, O. Devos ^c, M. Zakhour ^a, M. Nakhl ^a,
J.-L. Bobet ^{b,*}

^a LCPM/PR₂N (EDST), Lebanese University, Faculty of Sciences II, 90656, Jdeidet El Metn, Lebanon

^b University of Bordeaux, ICMCB, UMR 5026, F 33600 Pessac, France

^c University of Bordeaux, CNRS, Arts et Metiers Institute of technology, Bordeaux INP, INRAE, I2M Bordeaux, F 33400 Talence, France

H I G H L I G H T S

- Mg₁₇Al₁₂ corrodes in a 3.5 wt% aqueous solution of NaCl with a corrosion current density of 5.3 μA/cm².
 - Mg₁₇Al₁₂ can act as cathode in Mg-Al alloy with an OCP of -1.2 V/SCE.
 - Electrochemical impedance spectroscopy can explain the effect of ball milling additives.
 - Ball milling with MgCl₂ increases the corrosion current density by 22 times.
-

A R T I C L E I N F O

Article history:

Received 18 February 2020

Received in revised form

9 March 2020

Accepted 4 April 2020

Available online 1 May 2020

Keywords:

Mg₁₇Al₁₂

Corrosion

Mg-Al alloys

Electrochemical impedance

spectroscopy

Ball milling

Hydrogen

A B S T R A C T

The corrosion behavior of pure Mg₁₇Al₁₂ and the effect of ball milling in presence of additives (i.e. graphite (G) and magnesium chloride (MgCl₂)) are evaluated in 3.5 wt% NaCl aqueous solution using electrochemical polarization and impedance measurements. Pure Mg₁₇Al₁₂ and milled Mg₁₇Al₁₂ without additives and with MgCl₂ present an open current potential (OCP) of -1.2 V/SCE while Mg₁₇Al₁₂ + G shows a slightly higher OCP (+10% maximum). Mg₁₇Al₁₂ corrodes with low kinetics and an increase of corrosion rate for the milled Mg₁₇Al₁₂ is observed. The corrosion current densities (J_{corr}) derived from the Tafel plots, exhibit their corrosion reactivity as follow: Mg₁₇Al₁₂ < Mg₁₇Al₁₂ 5h < Mg₁₇Al₁₂ + G 5h < Mg₁₇Al₁₂ + MgCl₂ 5h. Electrochemical impedance spectroscopy (EIS) results are in good agreement with the measured J_{corr} . Randles circuit models are established for all samples to explain their surface behavior in the aqueous NaCl solution. The variation of the fitted parameters is attributed either to the effect of ball milling or to the effect of the additive. Our results are helpful in elucidating the effect of ball milling and the additives.

* Corresponding author.

E mail address: jean.louis.bobet@icmcb.cnrs.fr (J. L. Bobet).

Introduction

Magnesium alloys have become an important light weighting structural materials in various fields, such as electronic, automotive and aircraft industries, due to their high strength/weight ratios, low density, good conductivity and easy application recycling [1–5]. In spite of these superior properties, magnesium alloys are easily corroded in a corrosive environment, because of the high reactivity of Mg [6–10] and the instability of the protective film formed on the alloy surfaces [11]. Poor corrosion resistance of magnesium alloys has been one of the major obstacles to their extensive applications as structural materials. Among the magnesium alloys, AZ series magnesium alloys (i.e. Mg–Al–Zn alloys) are the most successfully used commercial alloys in the manufacturing industry. Nevertheless, their application is still limited due to their lower corrosion resistance compared to that of aluminum alloys.

According to ASTM coding [12], these alloys mainly contain – apart from Mg–Al and Zn where Al can form with Mg the intermetallic $Mg_{17}Al_{12}$ (commonly named β phase). The corrosion properties of the Mg–Al–Zn alloys have been previously studied by changing the stoichiometry of the alloying elements [13–15] to get better corrosion resistance. Nevertheless, for most of these alloys, other phases precipitate and can play an important role in the corrosion procedure of Mg substrate in various manner. Therefore, understanding the mechanism of the corrosion induced by these other phases is of great importance. The hydrolysis of magnesium based materials is an electrochemical reaction where Mg is oxidized to Mg^{2+} and water is reduced to produce H_2 gas [16]. Consequently, bad corrosion resistance lead to high production of hydrogen and using Mg–Al based wastes materials to produce H_2 by the hydrolysis reaction can offer a second life to these wastes.

The corrosion behavior of Mg alloys is mainly related to their microstructure. For Mg–Al–Zn alloys, two binary intermetallic compounds $MgZn$ and $Mg_{17}Al_{12}$, have been reported for their influence on the corrosion behavior. The β intermetallic ($Mg_{17}Al_{12}$), which precipitates at grain boundaries, is formed in Mg alloys containing more than 2% Al [17,18] and its morphology depends upon the volume fraction of Al [14,19,20], the solidification rate of the melt [21] and the minor alloying additions [22–26]. Several studies have focused on the corrosion of AZ series to better understand their corrosion mechanisms [14,17,19,27–31]. However, the controversial views on the role of Al in the corrosion of these alloys still exist depending on the amount of the β phase and so of the surface contact between the two phases. On one hand, the corrosion resistance of the magnesium alloy improves when aluminum content reaches 8%–9% due to protective barrier effect of $Mg_{17}Al_{12}$ promoted by Al content [27,32]. On the other hand, the intermetallic phase accelerates the overall corrosion of the alloy when aluminum content is about 2%–3% due to a micro galvanic cell system established between Mg and $Mg_{17}Al_{12}$ [14,17,30,31]. Cheng et al. [17] showed that the galvanic couples formed by the second phase particles and the matrix are the main source of the localized corrosion of magnesium alloys. Also, the microscopic corrosion morphology of the alloys had

strong relationship with the property and the distribution of the second phase particles. The corrosion resistance of AZ91 was reported to be lower than that of AZ31 due to the difference in aluminum content between the two alloys (inducing consequently a different of $Mg_{17}Al_{12}$ amount) where $Mg_{17}Al_{12}$ can form micro galvanic cell with the Mg matrix. Feng et al. [33] showed that β phase precipitates both along the grain boundaries and also in the Mg matrix. This last phase is playing the role of a cathodic phase, and then improves the corrosion dissolution of Mg substrate. Therefore, the corrosion close to the Mg matrix is strongly influence by the shape of this phase. In fact, the larger surface energy caused by the shape of the second phase, the higher corrosion reactivity and corrosion rate of the nearby Mg substrate. Zhao et al. [34] stated that $Mg_{17}Al_{12}$ can act as a corrosion barrier and hinder the corrosion propagation in the Mg matrix. So, the β phase has two roles: (i) a barrier when its fraction is relatively high and (ii) a galvanic cathode when it precipitates in the Mg matrix with a small volume fraction.

Our prior work [35] showed that pure as cast $Mg_{17}Al_{12}$ barely reacts with 3.5 wt% NaCl aqueous solution. We have shown that, after 1h of reaction, it generates only 6% of its theoretical H_2 generation capacity. Moreover, a minimum of 5 h duration ball milling duration is needed to decrease sufficiently its crystallites and particles size enhancing its hydrolysis performance. Ball milling with relatively cheap additives (i.e. graphite (G), sodium chloride (NaCl), magnesium chloride ($MgCl_2$) and aluminum chloride ($AlCl_3$)) was found to be beneficial on the hydrolysis of $Mg_{17}Al_{12}$. Although, the simultaneous addition of graphite and $AlCl_3$ demonstrated the highest hydrolysis performances (i.e. 16% of the theoretical H_2 generation after 1h).

In this work, corrosion behavior of pure $Mg_{17}Al_{12}$, $Mg_{17}Al_{12}$ ball milled for 5h and $Mg_{17}Al_{12}$ ball milled for 5h in presence of graphite (G) or magnesium chloride ($MgCl_2$) were studied by electrochemical measurements for improving hydrogen generation (i.e. corrosion reaction) of Mg based wastes materials. Our results clarify the barrier effect of $Mg_{17}Al_{12}$ during the corrosion AZ alloys and show that ball milling enhances the corrosion of $Mg_{17}Al_{12}$. Randles circuit for pure $Mg_{17}Al_{12}$ was established in order to highlight the role of ball milling and/or of additives (i.e. according to the variation of the calculated parameters).

Experimental procedure

The preparation details of all the pure materials and mixtures are detailed in Ref. [35]. $Mg_{17}Al_{12} + X$ 5h (X milling additive, i.e. G and $MgCl_2$) refers to $Mg_{17}Al_{12}$ ball milled with 5 wt% of additive X for 5h at 250 rpm. In addition, as always, instead of using real seawater, we used 3.5 wt% NaCl solution, which was prepared from analytical grade reagent and deionized water.

Open circuit potential (OCP), potentiodynamic polarization curve, and electrochemical impedance spectrum (EIS) were determined, using an electrochemical workstation (Ametek VersaSTAT 3F type) at room temperature in 3.5 wt% NaCl solution with a classical three electrode cell setup [described in Ref. [36]]. The counter electrode was a platinum foil and the

reference electrode was a saturated calomel electrode (SCE). The working electrode was a pellet made by cold pressing of 300 mg of our prepared powder in a 10 mm diameter stainless steel cylindrical die. A load of 5500 kg/cm² was applied during 3 min leading to a nearly fully dense pellet. The capsule was sealed by epoxy with an exposed area of approximately 0.80 cm² ± 0.20 cm² (measured using ImageJ software) and was wet ground with ethanol to a 4000 grit finish. OCP and potentiodynamic polarization tests were performed following the procedure reported in Ref. [36]. The EIS measurements were carried out over a frequency ranging from 100 kHz to 1 Hz with a 10 mV amplitude sinusoidal voltage at OCP. The EIS results were fitted using the commercial ZView 3.5f software. The fitting errors of the parameters are less than 5%. For better reproducibility, all above electrochemical measurements were repeated at least twice.

Note that in the case of Mg₁₇Al₁₂ ball milled 5h with AlCl₃, NaCl and G + AlCl₃, the anodic polarization tests could not be established because of the continuous chemical modification of both the materials surface and the electrolyte near the surface. This avoids the attenuation of a stable OCP required for both the anodic polarization tests and electrochemical impedance measurements.

Results and discussion

Open current potential

The Open Circuit Potential (OCP) variations as a function of time were recorded for pure Mg₁₇Al₁₂, Mg₁₇Al₁₂ 5h, Mg₁₇Al₁₂ + G 5h and Mg₁₇Al₁₂ + MgCl₂ 5h materials (Fig. 1).

The corrosion potentials were calculated from OCP measurements by averaging OCP values from 35 min to 60 min of immersion where the potential was the most stable. From these experimental results, it is found that pure Mg₁₇Al₁₂ shows slower stabilization kinetics as compared to the milled materials (*e.g.* the variation of the potential is negligible after 10 min of immersion) and the value of E_{corr} is of the order of

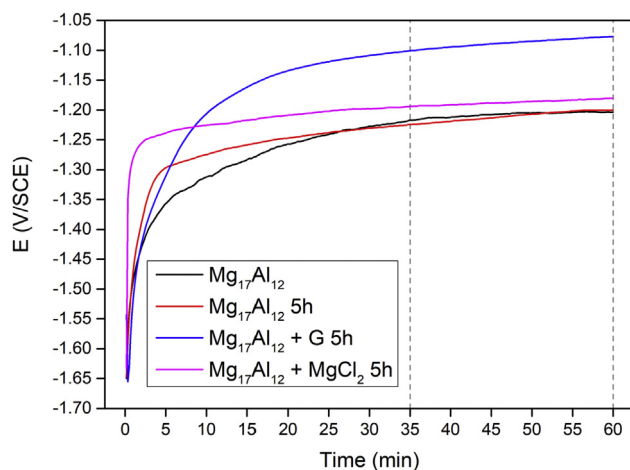


Fig. 1 – OCP measurement with immersion time, as a function of time for Mg₁₇Al₁₂, Mg₁₇Al₁₂ 5h, Mg₁₇Al₁₂ + G 5h and Mg₁₇Al₁₂ + MgCl₂ 5h in 3.5 wt% NaCl aqueous solution.

1.20 ± 0.05 V/SCE (Table 1). Our results confirm the galvanic coupling between Mg and Mg₁₇Al₁₂ since Mg₁₇Al₁₂ is more noble than Mg and the difference of corrosion potential is 0.45 V (OCP (Mg) 1.65 V/SCE [36]), which exceeds the 0.25 V required for galvanic coupling [36]. Thus, this potential difference accelerates the corrosion of Mg in Mg–Al alloys, where Mg₁₇Al₁₂ acts as cathode and Mg as anode [37].

Lunder *et al.* [27] reported that pure Mg₁₇Al₁₂ has an OCP of 1.20 V/SCE in 5 wt% NaCl. According to Pourbaix diagram of the magnesium water system [38], a hydroxide layer is formed on the surface of the alloys which prevents the anodic dissolution of the metal. It should be noted that the compound Mg(OH)₂ is, thermodynamically, the most stable formed compound during the immersion in water (or “model” seawater) even at the nanometric size [39]. With free potential, the anodic and cathodic reactions decrease as a function of the immersion time leading to the formation of a protective film on the metal surface. For pure Mg₁₇Al₁₂, the potential drifted from an initial value of 1.65 V/SCE up to about 1.2 V/SCE, suggests gradual passivation of the surface. Thus, the stabilization kinetics of the free potential may be indicative of the corrosion rate *e.g.* the passive layer is formed faster due to an increase in the corrosion kinetics. Note that in the case of Mg₁₇Al₁₂ + G 5h, the value of the OCP slightly increases (1.08 V/SCE) due to galvanic coupling between Mg₁₇Al₁₂ and graphite.

Corrosion rate

Anodic polarisation is a useful tool to characterise the dissolution of Mg materials as a function of the applied potential [40]. The corrosion current density (J_{corr}) of each material was determined from the anodic polarization curves (Fig. 2) and the Tafel plot [40]. The anodic polarisation curve of pure Mg₁₇Al₁₂ demonstrates the formation of a passive film that inhibits the corrosion from 20 mV/OCP up to 200 mV/OCP. The same behaviour (*i.e.* passivation layer formation) was observed previously for AZ alloys and Mg [41]. Our prior work [42] proved experimentally the formation of a MgO/Mg(OH)₂ layer on Mg₁₇Al₁₂ surface at 20 mV/OCP and the breakdown of this layer promoting the appearance of fresh Mg as the applied potential increases. Thus, the “barrier” effect of Mg₁₇Al₁₂ during the corrosion of Mg–Al alloys can be explained by the large difference in the corrosion kinetics between Mg and Mg₁₇Al₁₂ (558 μA/cm² [36] vs 5.3 μA/cm² respectively).

The reactivity, in term of corrosion kinetics, varies in the order: Mg₁₇Al₁₂ + MgCl₂ 5h > Mg₁₇Al₁₂ + G 5h > Mg₁₇Al₁₂ 5h > Mg₁₇Al₁₂ (Table 1 and Fig. 2). These results are in total agreement with those reported in our previous work [35]. Referring to Fig. 2, the passivity plateau increases in the order Mg₁₇Al₁₂ + MgCl₂ 5h < Mg₁₇Al₁₂ 5h < Mg₁₇Al₁₂ where in the case of Mg₁₇Al₁₂ + G 5h passivation phenomenon is less significant. This may be attributed to the formation of a fine graphite layer which prevents the adhesion of the formed MgO/Mg(OH)₂ on the surface [43,44].

Ball milling of Mg₁₇Al₁₂ allow increasing the number of microstructural defects and decreasing the particles size (*i.e.* the grain boundaries density is then increasing a lot) [35]. This play a concomitant role to enhance the pitting corrosion by the localized enrichment in chloride [45,46]. This is also

Table 1 – OCP values and corrosion current density (J_{corr}) for Mg [36], $Mg_{17}Al_{12}$, $Mg_{17}Al_{12}$ 5h, $Mg_{17}Al_{12}$ + G 5h and $Mg_{17}Al_{12}$ + $MgCl_2$ 5h.

Sample	Mg [36]	$Mg_{17}Al_{12}$	$Mg_{17}Al_{12}$ 5h	$Mg_{17}Al_{12}$ + G 5h	$Mg_{17}Al_{12}$ + $MgCl_2$ 5h
E_{corr} (V/SCE)	1.65 ± 0.1	1.20 ± 0.05	1.20 ± 0.05	1.08 ± 0.04	1.18 ± 0.05
J_{corr} ($\mu A/cm^2$)	558 ± 25	5.3 ± 0.05	90.6 ± 4.5	94.8 ± 5	116.1 ± 5.5

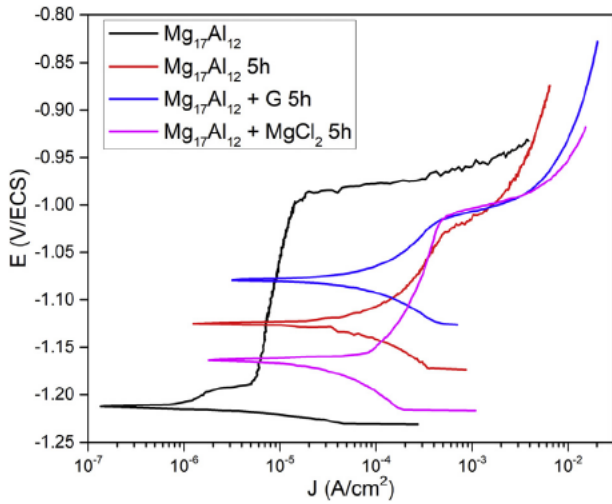


Fig. 2 – Anodic polarization curves for $Mg_{17}Al_{12}$, $Mg_{17}Al_{12}$ 5h, $Mg_{17}Al_{12}$ + G 5h and $Mg_{17}Al_{12}$ + $MgCl_2$ 5h in 3.5 wt% NaCl aqueous solution.

observed in Fig. 1 where $Mg_{17}Al_{12}$ 5h reaches a stable state (formation of an $MgO/Mg(OH)_2$ passive layer) after 10 min, while $Mg_{17}Al_{12}$ reaches this state after 30 min. The presence of structural defects in $Mg_{17}Al_{12}$ milled for 5h therefore accelerates its corrosion and the corrosion current density goes from $5.3 \mu A/cm^2$ (for unmilled $Mg_{17}Al_{12}$) to $90.6 \mu A/cm^2$ (Table 1 and Fig. 2).

As previously reported about the effect of $AlCl_3$, milling with $MgCl_2$ generates more microstructural defects (i.e. initiator sites). Also the dissolution of this salt which is highly exothermic allows preventing the formation of a continuous passive layer [35]. This leads to an increase of the corrosion current density from $90.6 \mu A/cm^2$ (for $Mg_{17}Al_{12}$ milled for 5h without $MgCl_2$) to $116.1 \mu A/cm^2$ (Table 1 and Fig. 2).

Electrochemical impedance spectroscopy (EIS)

Electrochemical impedance spectroscopy (EIS) is a powerful technique for investigating the electrical properties of a surface in combination with physicochemical processes [47]. Local electrochemical impedance spectroscopy (LEIS) was used to investigate the impedance of the phases in Mg–Al systems [48–50] but galvanic coupling between Mg and $Mg_{17}Al_{12}$ may affect the electrochemical behavior of each component. That's why EIS measurements were carried out at E_{corr} of each form of $Mg_{17}Al_{12}$ after 1h of immersion. The impedance data shown in Fig. 3 were adapted to the equivalent circuit shown in Fig. 4a.

The elements of equivalent circuit are as follows: (i) the aqueous solution resistance (R_s) is the resistance of the

electrolyte, (ii) the charge transfer or film resistance (R), (iii) the constant phase element (CPE) and (iv) the diffusion induced Warburg element (W_s).

R and CPE are linked by the equation: $C_{eff} R^{-1} (QR)^{1/\alpha}$ [50] where C_{eff} is the effective capacity, α ($0 < \alpha < 1$) reflects the surface impedance distribution and Q the CPE capacity. Depending on these last two parameters (i.e. α , Q), the CPE and R may present different physical explanation:

if $0 < \alpha < 0.5$, the CPE describes the diffusion through a porous film on the surface and R describes the corresponding diffusion resistance.

if $\alpha > 0.5$, the electrochemical reaction is the limiting process and the explanation of Q and R depends on the value of C_{eff} . If $C_{eff} < 10 \mu F/cm^2$, CPE is the oxide film capacitance and R its resistance; while if $C_{eff} > 10 \mu F/cm^2$, CPE is the capacitance of the double layer and R is the charge transfer resistance.

If $\alpha \approx 0.5$, the electrochemical reaction is kinetically favorable and the diffusion is the limiting process. In this case, the CPE and R doesn't have a physical meaning and should be replaced by a Warburg element (Fig. 4b)

The diffusion induced Warburg element is known as the finite space diffusion Warburg impedance. It represents the transition from Warburg behavior (45° line) to a capacitive behavior in the lower frequency range. The Warburg impedance depends on three parameters: R_w , T_w and β . R_w is the limiting diffusion resistance and depends on the concentration and the mobility [52]. T_w is the diffusion time constant ($T_w = L^2/D$ where L is the diffusion length or the film thickness and D the diffusion coefficient) [53]. β is an exponent related with the roughness of the diffusion media (an exponent of 0.5 means ideal Warburg diffusion, i.e. 45° line) [47,54].

EIS experimental data of all the materials involved in this study were fitted according to the equivalent circuit represented in Fig. 4a. For $Mg_{17}Al_{12}$ 5h and $Mg_{17}Al_{12}$ + $MgCl_2$ 5h, the values of α are respectively 0.49 and 0.52, the Q values are respectively $1138.5 \mu F/s^\alpha \cdot cm^2$ and $1131.1 \mu F/s^\alpha \cdot cm^2$ and the associated resistances R are respectively $47.4 \Omega/cm^2$ and $20 \Omega/cm^2$. As explicated previously, values of α of 0.5 indicates that the CPE has no physical meaning and the corrosion kinetics is thus limited by a diffusional phenomenon (higher the corrosion rate, lower the charge transfer resistance R). For these reasons, the values of α , Q and R for $Mg_{17}Al_{12}$ 5h and $Mg_{17}Al_{12}$ + $MgCl_2$ 5h will not be explicated when showing the calculated parameters values. Therefore, the impedance data of $Mg_{17}Al_{12}$ 5h and $Mg_{17}Al_{12}$ + $MgCl_2$ 5h were fitted with the equivalent circuit shown in Fig. 4b.

Table 2 shows the values of the various parameters calculated using as a function of the equivalent circuits represented in Fig. 4.

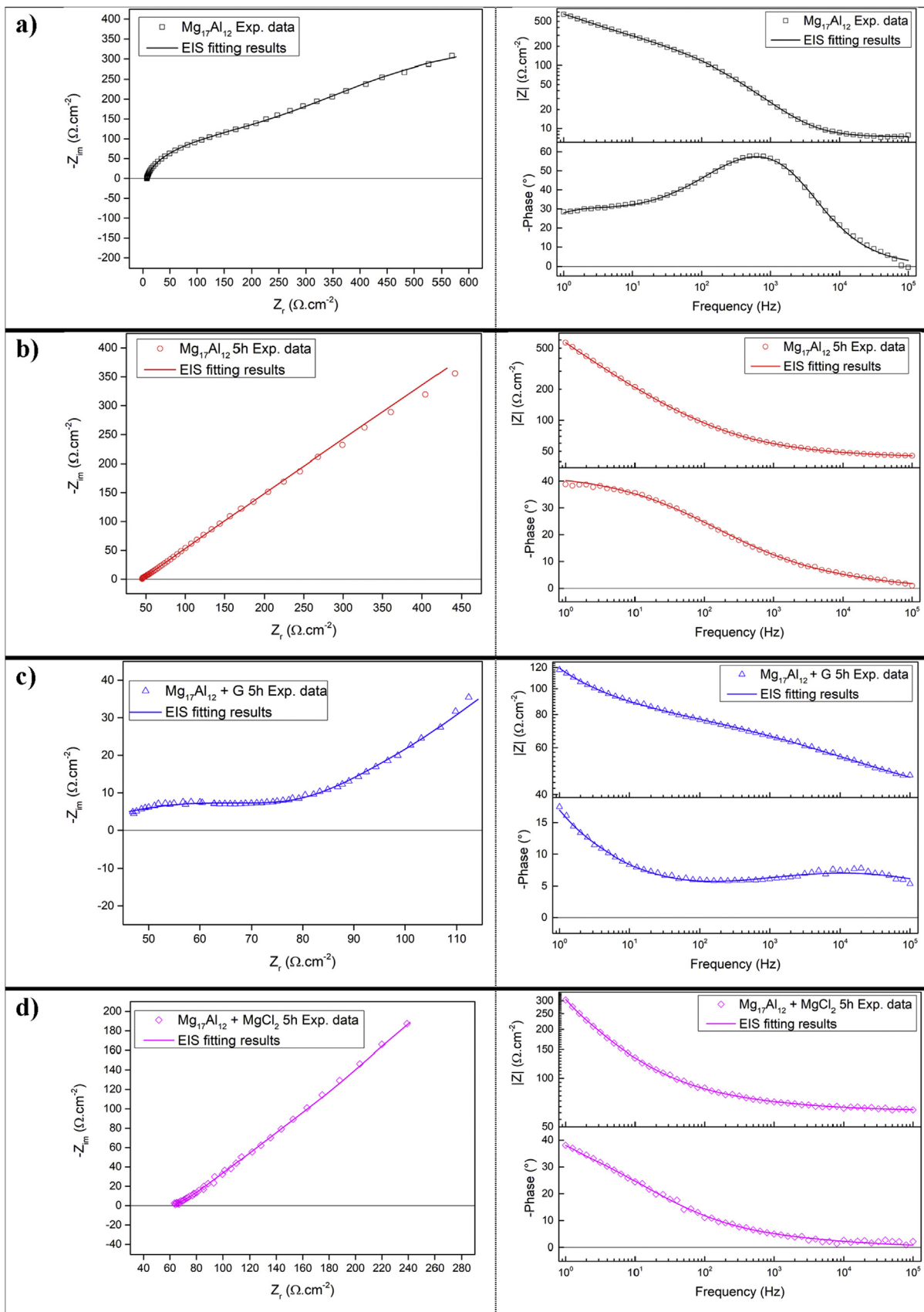


Fig. 3 – Nyquist (left) and Bode (right) plots for: (a) $Mg_{17}Al_{12}$, (b) $Mg_{17}Al_{12}$ 5h, (c) $Mg_{17}Al_{12} + G$ 5h and (d) $Mg_{17}Al_{12} + MgCl_2$ 5h.

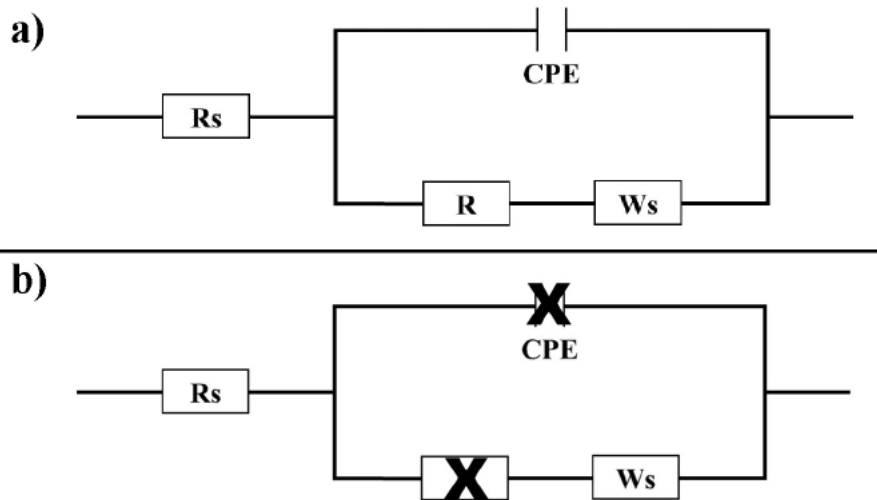


Fig. 4 – Electrical equivalent circuit used to interpret a) the impedance data in 100Khz - 1Hz range and b) the diffusion process (where R and CPE are insignificant).

The calculated α values (Table 2) confirm that ball milling accelerate the corrosion rate of $Mg_{17}Al_{12}$. α decreases from 0.92 for $Mg_{17}Al_{12}$ to approximately 0.5 for $Mg_{17}Al_{12}$ ball milled with $MgCl_2$ and without additives for 5h (therefore these last 2 materials are analyzed by equivalent circuit shown in Fig. 4b). Indeed, when corrosion kinetics increases, the time constant associated to charge transfer (i.e. electrochemical reaction) process decreases and the overall mechanism is limited by diffusion. For $Mg_{17}Al_{12} + G$ 5h, $\alpha < 0.5$, which indicates a diffusion process through a deposited surface layer that may confirm the formation of a graphite layer at the surface. Indeed, other authors showed that ball milling of Mg [43], WE43 [44] and $Mg_{17}Al_{12}$ [35] with graphite forms a fine graphite layer on the surface which favor the hydrolysis reaction by inhibiting the adhesion of $Mg(OH)_2$ on the surface. This is a new evidence on the role of graphite on the corrosion (implying hydrolysis) of Mg based materials.

The effective capacitance C_{eff} calculated for pure $Mg_{17}Al_{12}$ is greater than $10 \mu F/cm^2$ ($C_{eff} = 18 \mu F/cm^2$) indicating that the corresponding resistance is the charge transfer resistance. When the corrosion is fast, the passive film of $MgO/Mg(OH)_2$ is formed rapidly, its thickness will then be more important and

the exposed surface area of the materials will be higher (rough surface) compared to the passive film formed when slow kinetic corrosion occurred.

The charge transfer resistance R varies inversely with the surface area (while the surface area varies as the corrosion rate) [51] so the higher the corrosion rate, the lower R will be. Comparing pure $Mg_{17}Al_{12}$ and milled $Mg_{17}Al_{12}$, R is negligible compared to R_w indicating that ball milling with and without additives enhances the corrosion of $Mg_{17}Al_{12}$. These results are consistent with those previously mentioned (section Corrosion rate) and reported [35].

The diffusion limited corrosion can be studied by fitting the EIS results according to the equivalent circuit of Fig. 4b.

The first indication given by the model is that, after ball milling, the diffusion is a rate limiting process and cannot be neglected. This is highlighted by the higher values of R_w obtained after ball milling.

As the values of R_w and T_w are related to the effective diffusion thickness [54], it is the signature of a variation in corrosion layer thickness. As it appears that ball milling of $Mg_{17}Al_{12}$ increases both R_w and T_w (from $1404.9 \Omega/cm^2$ to

Table 2 – Electrochemical parameters, of equivalent circuits shown in Fig. 4a and 4b, obtained from best fit of impedance data.

Sample	$Mg_{17}Al_{12}^a$	$Mg_{17}Al_{12}$ 5h ^b	$Mg_{17}Al_{12} + G$ 5h ^a	$Mg_{17}Al_{12} + MgCl_2$ 5h ^b
R_s (Ω/cm^2)	7.0	44.1	36.7	62.9
CPE				
Q ($\mu F/s^\alpha \cdot cm^2$)	10.4	∞	675.4	∞
α	0.92	X	0.39	X
R (Ω/cm^2)	52.2	≈ 0	43.4	≈ 0
Warburg				
R_w (Ω/cm^2)	1405	3637	140	346
T_w (s)	2.3	8.4	1.5	0.4
β	0.33	0.49	0.43	0.47

^a Values are determined from fitting EIS data with the equivalent circuit shown in Fig. 4a.

^b Values are determined from fitting EIS data with the equivalent circuit shown in Fig. 4b.

3637.2 Ω/cm^2 and from 2.3 s to 8.4 s respectively, Cf Table 2), this indicates the thickening of the surface passivation layer.

For both $\text{Mg}_{17}\text{Al}_{12} + \text{G}$ 5h and $\text{Mg}_{17}\text{Al}_{12} + \text{MgCl}_2$ 5h, we observe a decrease of R_w and T_w which indicates for both a decrease of the thickness of the passivation layer. Nevertheless, the origin of the decrease is different. For $\text{Mg}_{17}\text{Al}_{12} + \text{G}$ 5h it is attributed to the formation of a graphite layer preventing the adhesion of $\text{Mg}(\text{OH})_2$ [42,43] and thus inhibiting the thickening of the passivation layer on the surface. For $\text{Mg}_{17}\text{Al}_{12} + \text{MgCl}_2$ 5h, it is attributed to the dissolution of the passivation layer formed due to the exothermic dissolution of MgCl_2 .

Conclusion

This work assessed the electrochemical behavior of intermetallic $\text{Mg}_{17}\text{Al}_{12}$ in 3.5 wt% NaCl aqueous solution. The OCP of $\text{Mg}_{17}\text{Al}_{12}$ intermetallic is more than 450 mV higher than that of pure magnesium, which verifies the galvanic coupling between Mg and $\text{Mg}_{17}\text{Al}_{12}$ in Mg–Al alloys. Moreover, the “barrier” effect, reported in the literature, can be clearly explained by the difference in corrosion rate between the various components of the alloys (e.g. Mg and $\text{Mg}_{17}\text{Al}_{12}$). Ball milling improves the corrosion of $\text{Mg}_{17}\text{Al}_{12}$ (anodic reaction) and simultaneously the hydrogen production (cathodic reaction). MgCl_2 addition provides the highest corrosion rate due to the exothermic dissolution of MgCl_2 in the medium that favor the destruction of the passivation layer.

The electrochemical properties of the materials during immersion in NaCl solution was investigated by electrochemical impedance spectroscopy. The proposed equivalent circuit, based on EIS measurements and fitting, explains the corrosion mechanism of the intermetallic in the aqueous NaCl solution and the role of additives. Corrosion of pure $\text{Mg}_{17}\text{Al}_{12}$ is limited by a charge transfer mechanism (i.e. electrochemical reaction) indicating that the corrosion of the intermetallic is relatively low. From the general equivalent circuit and based on the fitted parameters, a sub model was established, by neglecting the contribution of R and the CPE, in order to qualify the effect of additives. For the intermetallic milled with and without additives (i.e. graphite and MgCl_2), the corrosion rate increases and the corrosion mechanism is diffusive. When corrosion rate increases, the charge transfer resistance decreases and become negligible which justify the transition from a charge transfer limited mechanism to a diffusive mechanism. The values of the Warburg parameters (i.e. R_w and T_w), from the sub model 1, allow the clarification of the role of each additive:

- (i) the formation of a graphite layer during ball milling of $\text{Mg}_{17}\text{Al}_{12}$ (this phenomenon is identified owing to the diffusion through a porous film on the surface) and
- (ii) the dissolution of the passivation layer formed following the exothermic dissolution of MgCl_2 (this phenomenon is identified owing to the thinning of the passivation layer).

We have shown that electrochemical impedance spectroscopy is an effective tool for studying the corrosion of

milled materials. Moreover, it shows the advantage of explaining the effect of ball milling additives, especially those based on Mg when compared to anodic polarization technic.

5. Acknowledgments

This work was financially supported by the AZM & SAADE Association, the Lebanese University and Bordeaux foundation, France. Authors also thank Prof. Fabrice Mauvy for valuable discussion and for assistance with EIS fitting.

Appendix A. Supplementary data

Supplementary data to this article can be found online at <https://doi.org/10.1016/j.ijhydene.2020.04.030>.

REFERENCES

- [1] Mordike BL, Ebert T. Magnesium: properties applications potential. *Mater Sci Eng* 2001;302:37–45. [https://doi.org/10.1016/S0921-5093\(00\)01351-4](https://doi.org/10.1016/S0921-5093(00)01351-4).
- [2] Udhayan R, Bhatt DP. On the corrosion behaviour of magnesium and its alloys using electrochemical techniques. *J Power Sources* 1996;63:103–7. [https://doi.org/10.1016/S0378-7753\(96\)02456-1](https://doi.org/10.1016/S0378-7753(96)02456-1).
- [3] Friedrich H, Schumann S. Research for a “new age of magnesium” in the automotive industry. *J Mater Process Technol* 2001;117:276–81. [https://doi.org/10.1016/S0924-0136\(01\)00780-4](https://doi.org/10.1016/S0924-0136(01)00780-4).
- [4] Kulekci MK. Magnesium and its alloys applications in automotive industry. *Int J Adv Manuf Technol* 2008;39:851–65. <https://doi.org/10.1007/s00170-007-1279-2>.
- [5] Aghion E, Bronfin B, Eliezer D. The role of the magnesium industry in protecting the environment. *J Mater Process Technol* 2001;117:381–5. [https://doi.org/10.1016/S0924-0136\(01\)00779-8](https://doi.org/10.1016/S0924-0136(01)00779-8).
- [6] Liu LJ, Schlesinger M. Corrosion of magnesium and its alloys. *Corrosion Sci* 2009;51:1733–7. <https://doi.org/10.1016/j.corsci.2009.04.025>.
- [7] Pardo A, Merino MC, Coy AE, Arrabal R, Viejo F, Matykina E. Corrosion behaviour of magnesium/aluminium alloys in 3.5wt.% NaCl. *Corrosion Sci* 2008;50:823–34. <https://doi.org/10.1016/j.corsci.2007.11.005>.
- [8] Song G, Atrens A, John DS, Wu X, Nairn J. The anodic dissolution of magnesium in chloride and sulphate solutions. *Corrosion Sci* 1997;39:1981–2004. [https://doi.org/10.1016/S0010-938X\(97\)00090-5](https://doi.org/10.1016/S0010-938X(97)00090-5).
- [9] Song G, Atrens A, Stjohn D, Nairn J, Li Y. The electrochemical corrosion of pure magnesium in 1 N NaCl. *Corrosion Sci* 1997;39:855–75. [https://doi.org/10.1016/S0010-938X\(96\)00172-2](https://doi.org/10.1016/S0010-938X(96)00172-2).
- [10] Shi Z, Liu M, Atrens A. Measurement of the corrosion rate of magnesium alloys using Tafel extrapolation. *Corrosion Sci* 2010;52:579–88. <https://doi.org/10.1016/j.corsci.2009.10.016>.
- [11] Hara N, Kobayashi Y, Kagaya D, Akao N. Formation and breakdown of surface films on magnesium and its alloys in aqueous solutions. *Corrosion Sci* 2007;49:166–75. <https://doi.org/10.1016/j.corsci.2006.05.033>.
- [12] ASTM. Standard practice for codification of certain nonferrous metals and alloys, cast and wrought. West Conshohocken: ASTM International; 2005.

- [13] Meng C, Zhang D, Cui H, Zhuang L, Zhang J. Mechanical properties, intergranular corrosion behavior and microstructure of Zn modified Al Mg alloys. *J Alloys Compd* 2014;617:925–32. <https://doi.org/10.1016/j.jallcom.2014.08.099>.
- [14] Song G, Atrens A, Wu X, Zhang B. Corrosion behaviour of AZ21, AZ501 and AZ91 in sodium chloride. *Corrosion Sci* 1998;40:1769–91. [https://doi.org/10.1016/S0010-938X\(98\)00078-X](https://doi.org/10.1016/S0010-938X(98)00078-X).
- [15] Nam ND, Mathesh M, Le TV, Nguyen HT. Corrosion behavior of Mg–5Al–xZn alloys in 3.5wt.% NaCl solution. *J Alloys Compd* 2014;616:662–8. <https://doi.org/10.1016/j.jallcom.2014.07.014>.
- [16] Uan J Y, Yu S H, Lin M C, Chen L F, Lin H I. Evolution of hydrogen from magnesium alloy scraps in citric acid added seawater without catalyst. *Int J Hydrogen Energy* 2009;34:6137–42.
- [17] Cheng Y L, Qin T w, Wang H m, Zhang Z. Comparison of corrosion behaviors of AZ31, AZ91, AM60 and ZK60 magnesium alloys. *Trans Nonferrous Metals Soc China* 2009;19:517–24. [https://doi.org/10.1016/S1003-6326\(08\)60305-2](https://doi.org/10.1016/S1003-6326(08)60305-2).
- [18] Pekguleryuz M. Alloying behavior of magnesium and alloy design. In: Pekguleryuz MO, Kainer KU, Arslan Kaya A, editors. *Fundamentals of magnesium alloy metallurgy*. Woodhead Publishing; 2013. p. 152–96.
- [19] Pardo A, Merino MC, Coy AE, Viejo F, Arrabal R, Feliú S. Influence of microstructure and composition on the corrosion behaviour of Mg/Al alloys in chloride media. *Electrochim Acta* 2008;53:7890–902. <https://doi.org/10.1016/j.electacta.2008.06.001>.
- [20] Candan S, Candan E. A comparative study on corrosion of Mg–Al–Si alloys. *Trans Nonferrous Metals Soc China* 2017;27:1725–34. [https://doi.org/10.1016/S1003-6326\(17\)60195-X](https://doi.org/10.1016/S1003-6326(17)60195-X).
- [21] Candan S, Celik M, Candan E. Effectiveness of Ti micro alloying in relation to cooling rate on corrosion of AZ91 Mg alloy. *J Alloys Compd* 2016;672:197–203. <https://doi.org/10.1016/j.jallcom.2016.02.043>.
- [22] Candan S, Unal M, Turkmen M, Koc E, Turen Y, Candan E. Improvement of mechanical and corrosion properties of magnesium alloy by lead addition. *Mater Sci Eng* 2009;501:115–8. <https://doi.org/10.1016/j.msea.2008.09.068>.
- [23] Zeng R c, Zhang J, Huang W j, Dietzel W, Kainer KU, Blawert C, et al. Review of studies on corrosion of magnesium alloys. *Trans Nonferrous Metals Soc China* 2006;16:s763–71. [https://doi.org/10.1016/S1003-6326\(06\)60297-5](https://doi.org/10.1016/S1003-6326(06)60297-5).
- [24] Candan S, Unal M, Koc E, Turen Y, Candan E. Effects of titanium addition on mechanical and corrosion behaviours of AZ91 magnesium alloy. *J Alloys Compd* 2011;509:1958–63. <https://doi.org/10.1016/j.jallcom.2010.10.100>.
- [25] Choi HY, Kim WJ. The improvement of corrosion resistance of AZ91 magnesium alloy through development of dense and tight network structure of Al rich α phase by addition of a trace amount of Ti. *J Alloys Compd* 2017;696:736–45. <https://doi.org/10.1016/j.jallcom.2016.11.215>.
- [26] Gusieva K, Davies CHJ, Scully JR, Birbilis N. Corrosion of magnesium alloys: the role of alloying. *Int Mater Rev* 2015;60:169–94. <https://doi.org/10.1179/1743280414Y.0000000046>.
- [27] Lunder O, Lein JE, Aune TK, Nisancioglu K. The role of Mg₁₇Al₁₂ phase in the corrosion of Mg alloy AZ91. *Corrosion* 1989;45:741–8. <https://doi.org/10.5006/1.3585029>.
- [28] Salman SA, Ichino R, Okido M. A comparative electrochemical study of AZ31 and AZ91 magnesium alloy. *Int J Corrosion* 2010;2010. <https://doi.org/10.1155/2010/412129>.
- [29] Wang L, Shinohara T, Zhang B P. Electrochemical behaviour of AZ61 magnesium alloy in dilute NaCl solutions. *Mater Des* 2012;33:345–9. <https://doi.org/10.1016/j.matdes.2011.02.019>.
- [30] Samaniego A, Llorente I, Feliu S. Combined effect of composition and surface condition on corrosion behaviour of magnesium alloys AZ31 and AZ61. *Corrosion Sci* 2013;68:66–71. <https://doi.org/10.1016/j.corsci.2012.10.034>.
- [31] Singh IB, Singh M, Das S. A comparative corrosion behavior of Mg, AZ31 and AZ91 alloys in 3.5% NaCl solution. *J Magnes Alloys* 2015;3:142–8. <https://doi.org/10.1016/j.jma.2015.02.004>.
- [32] Froes FH, Kim Y W, Hehmann F. Rapid solidification of Al, Mg and Ti. *JOM* 1987;39:14–21. <https://doi.org/10.1007/BF03258603>.
- [33] Feng H, Liu S, Du Y, Lei T, Zeng R, Yuan T. Effect of the second phases on corrosion behavior of the Mg–Al–Zn alloys. *J Alloys Compd* 2017;695:2330–8. <https://doi.org/10.1016/j.jallcom.2016.11.100>.
- [34] Zhao MC, Uggowitz P, Liu M, Schmutz P, Song G, Atrens A. Corrosion of AZ91 – influence of the β phase morphology. *Mater Sci Forum* 2009;618–619:473–8. <https://doi.org/10.4028/www.scientific.net/MSF.618-619.473>.
- [35] Al Bacha S, Zakhour M, Nakhl M, Bobet JL. Effect of ball milling in presence of additives (Graphite, AlCl₃, MgCl₂ and NaCl) on the hydrolysis performances of Mg₁₇Al₁₂. *Int J Hydrogen Energy* 2020;45:6102–9. <https://doi.org/10.1016/j.ijhydene.2019.12.162>.
- [36] Alasmar E, Aubert I, Durand A, Nakhl M, Zakhour M, Gaudin E, et al. Hydrogen generation from MgNdNiMg15 composites by hydrolysis reaction. *Int J Hydrogen Energy* 2019;44:523–30. <https://doi.org/10.1016/j.ijhydene.2018.10.233>.
- [37] Südholz A, Kirkland N, Buchheit R, Birbilis N. Electrochemical properties of intermetallic phases and common impurity elements in magnesium alloys. *Electrochim Solid State Lett* 2011;14:C5–7. <https://doi.org/10.1149/1.3523229>.
- [38] Pourbaix M. *Atlas of electrochemical equilibria in aqueous solutions*. Houston, Texas, USA: NATIONAL ASSOCIATION of CORROSION ENGINEERS; 1974.
- [39] Ghanbari D, Salavati Niasari M, Sabet M. Preparation of flower like magnesium hydroxide nanostructure and its influence on the thermal stability of poly vinyl acetate and poly vinyl alcohol. *Compos B Eng* 2013;45(1):550–5. <https://doi.org/10.1016/j.compositesb.2012.09.007>.
- [40] Esmaily M, Svensson JE, Fajardo S, Birbilis N, Frankel GS, Virtanen S, et al. Fundamentals and advances in magnesium alloy corrosion. *Prog Mater Sci* 2017;89:92–193. <https://doi.org/10.1016/j.pmatsci.2017.04.011>.
- [41] Anik M, Avci P, Tanverdi A, Celikyurek I, Baksan B, Gurler R. Effect of the eutectic phase mixture on the anodic behavior of alloy AZ91. *Mater Des* 2006;27:347–55. <https://doi.org/10.1016/j.matdes.2004.11.016>.
- [42] Al Bacha S, Desmedt A, Bobet JL. Experimental evidence of H₂ spillover during the corrosion of Mg₁₇Al₁₂. Submitted to *Energy & Fuels*.
- [43] Awad AS, El Asmar E, Tayeh T, Mauvy F, Nakhl M, Zakhour M, et al. Effect of carbons (G and CFs), TM (Ni, Fe and Al) and oxides (Nb₂O₅ and V₂O₅) on hydrogen generation from ball milled Mg based hydrolysis reaction for fuel cell. *Energy* 2016;95:175–86. <https://doi.org/10.1016/j.energy.2015.12.004>.
- [44] Al Bacha S, Awad AS, El Asmar E, Tayeh T, Bobet JL, Nakhl M, et al. Hydrogen generation via hydrolysis of ball milled WE43 magnesium waste. *Int J Hydrogen Energy* 2019;44:17515–24. <https://doi.org/10.1016/j.ijhydene.2019.05.123>.
- [45] Li S L, Lin H M, Uan J Y. Production of an Mg/Mg₂Ni lamellar composite for generating H₂ and the recycling of the post H₂ generation residue to nickel powder. *Int J Hydrogen Energy* 2013;38:13520–8. <https://doi.org/10.1016/j.ijhydene.2013.08.051>.

- [46] Grosjean MH, Zidoune M, Roué L. Hydrogen production from highly corroding Mg based materials elaborated by ball milling. *J Alloys Compd* 2005;404:406-712. <https://doi.org/10.1016/j.jallcom.2004.10.098>.
- [47] Nguyen TQ, Breitung C. Determination of diffusion coefficients using impedance spectroscopy data. *J Electrochem Soc* 2018;165:E826-31. <https://doi.org/10.1149/2.1151814jes>.
- [48] Lacroix L, Blanc C, Pèbère N, Tribollet B, Vivier V. Localized approach to galvanic coupling in an aluminum-magnesium system. *J Electrochem Soc* 2009;156:C259-65. <https://doi.org/10.1149/1.3148833>.
- [49] Matthew Asmussen R, Jeffrey Binns W, Jakupi P, Shoesmith D. Microstructural effects on corrosion of AM50 magnesium alloys. *J Electrochem Soc* 2014;161:C501-8. <https://doi.org/10.1149/2.0781410jes>.
- [50] Baril G, Blanc C, Keddari M, Pèbère N. Local electrochemical impedance spectroscopy applied to the corrosion behavior of an AZ91 magnesium alloy. *J Electrochem Soc* 2003;150:B488-93. <https://doi.org/10.1149/1.1602080>.
- [51] Córdoba Torres P. Relationship between constant phase element (CPE) parameters and physical properties of films with a distributed resistivity. *Electrochim Acta* 2017;225:592-604. <https://doi.org/10.1016/j.electacta.2016.12.087>.
- [52] Bessler WG. A new computational approach for SOFC impedance from detailed electrochemical reaction-diffusion models. *Solid State Ionics* 2005;176:997-1011. <https://doi.org/10.1016/j.ssi.2005.01.002>.
- [53] Criado C, Galán Montenegro P, Velásquez P, Ramos Barrado JR. Diffusion with general boundary conditions in electrochemical systems. *J Electroanal Chem* 2000;488:59-63. [https://doi.org/10.1016/S0022-0728\(00\)00188-1](https://doi.org/10.1016/S0022-0728(00)00188-1).
- [54] Encinas Sánchez V, de Miguel MT, Lasanta MI, García Martín G, Pérez FJ. Electrochemical impedance spectroscopy (EIS): an efficient technique for monitoring corrosion processes in molten salt environments in CSP applications. *Sol Energy Mater Sol Cell* 2019;191:157-63. <https://doi.org/10.1016/j.solmat.2018.11.007>.